Food Chemistry 347 (2021) 128973

Contents lists available at ScienceDirect

Food Chemistry

journal homepage: www.elsevier.com/locate/foodchem

Cloning, purification and characterisation of cytosolic fructose-1,6-bisphosphatase from mung bean (*Vigna radiata*)

Lin Chen [a,b], Xue Zhao [a,b], Yun He [a,b], Hongshun Yang [a,b,*]

[a] Department of Food Science and Technology, National University of Singapore, Singapore 117542, Singapore
[b] National University of Singapore (Suzhou) Research Institute, 377 Lin Quan Street, Suzhou Industrial Park, Suzhou, Jiangsu 215123, PR China

ARTICLE INFO

Keywords:
Enzymatic properties
Vegetable
Energy metabolism
Site-directed mutagenesis
Molecular docking
Simulation

ABSTRACT

To improve the crop yield and quality, the cytosolic fructose-1,6-bisphosphatase (cFBPase) from mung bean (*Vigna radiata*), a rate-limiting enzyme in gluconeogenesis, was cloned, purified, and structurally characterised. To function it required Mg^{2+} and Mn^{2+} at 0.01–10 mM. The Michaelis-Menton constant and adenosine monophosphate (AMP) inhibitory constant (K_i) were 7.96 and 111.09 μM, respectively. The functional site residues of AMP binding (Arg^{30}, Asp^{32}, and Phe^{33}) and the active site residues (Asn^{218} and Met^{251}) were tested via site-directed mutagenesis and molecular docking. Asn^{218} and Met^{251} were replaced by Tyr and Leu, respectively. The M251L mutant showed enhanced substrate affinity and activity, resulting from decreased binding energy (–2.58 kcal·mol^{-1}) and molecular distance (4.2 Å). AMP binding site mutations changed the enzyme activities, indicating a connection between the binding and active sites. Furthermore, K_i and docking analysis revealed that Asp^{32} plays a key role in maintaining the AMP binding conformation.

1. Introduction

Fructose-1,6-bisphosphatase (FBPase) is a rate-limiting enzyme in gluconeogenesis, catalysing the irreversible conversion of the substrate fructose-1,6-bisphosphate (F16BP) into fructose-6-phosphate. It is also involved in many other metabolic pathways, such as the Calvin cycle and starch biosynthesis (Kuznetsova et al., 2010). Based on their amino acid sequences, FBPases are generally divided into five classes (type I–V). Type I, II, and III are typically found in bacteria, and type IV is more common to archaea. Type V exists in thermophiles from both domains. Moreover, eukaryotes are known to only contain the type I FBPases (Kuznetsova et al., 2010). Commonly, divalent metal ions, such as Mg^{2+} or Mn^{2+}, are required for FBPases' activities. In addition, their activities are regulated by adenosine monophosphate (AMP), phosphoenolpyruvate, and fructose 2,6-bisphosphate (Gao, Shen, & Honzatko, 2014).

In plants, at least two distinct FBPase isozymes exist (Ogawa et al., 2015). One is located in the chloroplasts stroma (chloroplastic FBPase, cpFBPase), which acts as a key regulator of the Calvin cycle by taking part in the production of ribulose-l,5-bisphosphate, an acceptor of CO_2 fixation. (Ozaki et al., 2009). Numerous studies have been performed to understand the regulatory role of cpFBPases in the photosynthetic rate, and plant growth and development because of their important functions in starch biosynthesis and photosynthesis (Rojas-González et al., 2015). Moreover, the crystal structure of spinach cpFBPase showed that the active site residues are conserved compared with those in pig kidney FBPase. However, the AMP binding site residues are not conserved and are located between three helixes (H1, H2, and H3) and a β-sheet (Villeret, Huang, Zhang, Xue, & Lipscomb, 1995).

The other plant FBPase is related to the gluconeogenesis and sucrose metabolism, being present in the cytoplasm (cytosolic FBPase, cFBPase) (Gütle et al., 2016). cFBPase controls the rate of triose phosphates withdrawal from the chloroplast. Whole genome sequencing of various plants provided information on the gene sequences of cFBPase. In *Arabidopsis*, cFBPase shares 50% sequence identity with cpFBPase, implying that the two isozymes may have evolved from the same origin (Kuznetsova et al., 2010). Recent studies investigated the physiological functions of cFBPases in plants. For instance, the overexpression of cytosolic *FBP* in tobacco improved the leaf number, fresh weight, photosynthetic activity, and conversion efficiency of hexose to sucrose (Tamoi et al., 2011). Moreover, the structural properties of cFBPases are different to those of cpFBPase. For instance, a unique domain related to light regulation is inserted in cpFBPase, while cFBPase is not regulated by light (Daie, 1993). However, to date, much less is known about

* Corresponding author at: Department of Food Science and Technology, National University of Singapore, Singapore 117542, Singapore.
E-mail address: fstynghs@nus.edu.sg (H. Yang).

https://doi.org/10.1016/j.foodchem.2020.128973
Received 1 April 2020; Received in revised form 26 November 2020; Accepted 28 December 2020
Available online 4 January 2021
0308-8146/

cFBPase (neither its transcriptional regulation nor its protein structure) compared with the extensively studied cpFBPase.

Our previous studies showed that during the germination of mung bean, positive energy regulation [exogenous adenosine triphosphate (ATP) treatment] significantly increased the energy status and eventually improved the yield and quality of mung bean sprouts. ATP treatment significantly increased the transcriptional expression of fructose-1,6-bisphosphatase gene *in Vigna radiate* (*VrFBP)* by around 50-fold, indicating its important role in energy metabolism (Chen, Tan, Zhao, Yang, & Yang, 2019; Chen et al., 2019). As a key regulatory factor in energy metabolism and quality control, *FBP* could be a modification target in the mung bean genome for precision crop breeding. Therefore, the goals of this research were to understand the cFBPase's enzymatic and structural characteristics to improve the enzyme activity and substrate affinity. In addition, this work could provide valuable reference information for *FBP* editing in other crops to enhance their yield and quality. In the present study, the cytosolic *FBP* of mung bean was cloned and expressed. The cFBPase protein was further purified and characterised. In addition, the functions of certain active site residues were tested using site-directed mutation and molecular docking.

2. Materials and methods

2.1. TA cloning of the coding sequence of cFBPase from mung bean

The total RNA of mung bean was extracted according to our previously published method (Chen et al., 2019). The quality and concentration of the RNA were tested using a spectrophotometer (BioDrop, Biochrom, Cambridge, UK). Agarose gel [1% (w/v)] electrophoresis was applied to assess the RNA integrity. Thereafter, a First Strand cDNA Synthesis Kit (Promega Corporation, Madison, WI, USA) was used to synthesise cDNA from 2 μg of prepared RNA. The coding sequence (CDS) of target cytosolic *VrFBP* was amplified from the cDNA using high-fidelity (HF) *Pfu* DNA polymerase (Promega Corporation, Madison, WI, USA) and specific primers (WT-F and WT-R, Table S1) designed based on the whole genome sequence of mung bean (Kang et al., 2014). The PCR product was verified by electrophoresis and further purified using a DNA cleanup kit (New England Biolabs, Beverly, MA, USA). The obtained DNA fragment was inserted into the pGEM®-T Easy Vector (Promega Corporation, Madison, WI, USA) and transformed into the *Escherichia coli* DH5α competent cells (Thermo Fisher Scientific, San Jose, CA, USA) according to the manufacturer's instructions. After blue-white selection on agar plates, the positive clones were cultured and the recombinant plasmid (pG-VrFBP) were extracted using a GeneJET Plasmid Miniprep Kit (Thermo Fisher Scientific, San Jose, CA, USA), and sequenced by Bio Basic Asia Pacific Pte Ltd. (Singapore).

2.2. Bioinformatic analysis of cFBPase from mung bean

The sequence of *VrFBP* was submitted to the NCBI GenBank database and the gene sequence was analysed using the Basic Local Alignment Search Tool (BLAST) (https://blast.ncbi.nlm.nih.gov/Blast.cgi). Based on the alignment results, a phylogenetic tree was generated using MEGA 7 (Pennsylvania State University, PA, USA). In addition, several typical FBPase amino acid sequences, from *Vigna radiata*, *Glycine* max, *Ricinus communis*, *Solanum tuberosum*, *Arabidopsis thaliana*, *Oryza sativa*, *Spinacia oleracea*, *Escherichia coli*, and *Homo sapiens*, were selected to perform multiple alignments using ClustalX (Conway Institute, Dublin, Ireland). The tertiary structure of mung bean cFBPase was predicted using the online I-TASSER service (http://zhanglab.ccmb.med.umich.edu/I-TASSER/) and verified using a Ramachandran plot and Verify-3D (https://servicesn.mbi.ucla.edu/SAVES/) (Cheng et al., 2012). Furthermore, the properties of the deduced polypeptide (isoelectric point, molecular weight, stability index, and signal peptide) were calculated using ExPasy proteomics Server (http://web.expasy.org/). Lastly, the subcellular localisation was predicted using PSORT Prediction (http://psort1.hgc.jp/form.html).

2.3. Recombinant expression and purification of cFBPase

The putative *VrFBP* was further amplified by PCR using HF *Pfu* polymerase (Promega Corporation, Madison, WI, USA), with the extracted plasmid pG-VrFBP as the template, and specific primers with restriction endonuclease sites (WT-F-*Nde*I, WT-R-*Bam*HI, Table S1). The PCR product was analysed by electrophoresis, and the appropriate band was extracted from gel (GeneJET Gel Extraction Kit, Thermo Fisher Scientific, San Jose, CA, USA) and purified using a DNA cleanup kit (New England Biolabs, Beverly, MA, USA). The obtained DNA fragment and Pet 32a(+) vector (Novagen, Madison, WI, USA) were double digested by *Nde*I and *Bam*HI (New England Biolabs, Beverly, MA, USA). The digestion products were ligated using T4 DNA ligase (Promega Corporation, Madison, WI, USA) and transformed into DH5α competent cells. Twenty clones were randomly picked and the inserted gene was amplified using colony PCR. The PCR products were further checked by electrophoresis. Five clones with the appropriate band were selected and the recombinant plasmids were extracted and sequenced, respectively. The clone with correct recombinant plasmid was screened and the plasmid (Pet32-FBP) from the selected clone was transformed into the expression strain *E. coli* BL21 (DE3).

The recombinant DE3 were cultured in Luria–Bertani broth with 50 μg/mL ampicillin at 37 °C until the culture reached the exponential growth stage (OD600 ≈ 0.5). After that, the culture was cooled to 25 °C and the expression of cFBPase was induced by the addition of 0.1 mM isopropyl-*β*-D-thiogalactopyranoside (IPTG, Thermo Fisher Scientific, San Jose, CA, USA) for 9 h. The cells were harvested by centrifugation (8,000 × *g*, 10 min, 4 °C) and the pellet was resuspended in buffer [50 mM Tris-HCl (pH 7.5), 3 mM ascorbic acid, 1 mM dithiothreitol, 10% (v/v) glycerol, and 0.5% Triton X-100]. The crude enzyme was extracted by sonication in an ice bath after the addition of 1 mM protease inhibitor phenylmethanesulphonyl fluoride. The obtained soluble fraction was loaded onto a DEAE-Sepharose Fast Flow (Amersham Biosciences, Uppsala, Sweden) column and then a Sephacryl S-200 high-resolution (Amersham Biosciences, Uppsala, Sweden) gel-filtration column. The separated protein fractions were pooled and concentrated (Meng, Shen, Yang, Zhang, & Sheng, 2014). The purified protein solution was quantified by the Bradford method (Bio-Rad, Hercules, CA, USA).

During the expression and purification processes, sodium dodecyl sulphate polyacrylamide gel electrophoresis (SDS-PAGE) was applied to identify the proteins. The protein electrophoresis chamber system, 4–20% precast polyacrylamide gels, protein standard marker (10 to 250 kDa), SDS-PAGE running buffer, loading buffer, gel staining solution (Coomassie Brilliant Blue R-250), and destaining solution were purchased from Bio-Rad (Hercules, CA, USA). Around 10 μg of protein was loaded into each well of the gradient gel. Electrophoresis was performed at 80 V for approximately 120 min, followed by gel staining (1 h), and destaining (overnight) processes. The gel images were captured using gel imaging system G: BOX EF2 (Syngene, Synoptics Ltd., Cambridge, UK).

2.4. Enzyme assay and kinetic analysis

The activity of mung bean cFBPase was determined by measuring the increase in absorbance of the produced reduced nicotinamide adenine dinucleotide phosphate (NADPH) at 340 nm in a 1 mL mixture [50 mM Tris-HCl (pH 7.5), 10 mM $MgCl_2$, 0.5 mM $NADP^+$, 50 μM F16BP, 1 unit of glucose-6-phosphate dehydrogenase (Sigma-Aldrich, St. Louis, MO, USA), and 1 unit of phosphoglucose isomerase (Sigma-Aldrich, St. Louis, MO, USA)] using a UV-1800 spectrophotometer (Shimadzu Inc., Kyoto, Japan). The reaction was started by adding 1.5 μg of cFBPase into the mixture and the absorbance was monitored for 5 min at room temperature (Yuan et al., 2017). To test the metal requirement of cFBPase activity, 10 mM $MgCl_2$ in the 1 mL reaction mixture mentioned above was

replaced by Tris-HCl (control, 50 mM), $CaCl_2$, $CoCl_2$, $CuCl_2$, $MgCl_2$, $MnCl_2$, and $ZnCl_2$, respectively. The final concentrations of each divalent metal cation were set at 0.01, 0.1, 1, and 10 mM.

The Michaelis-Menton constant (K_m) values of the required divalent metal ions (Mn^{2+} and Mg^{2+}) for cFBPase activity were determined by measuring the enzyme activities with different concentrations of metal ions. Furthermore, the heat stability of cFBPase was tested by incubating the enzyme at different temperatures (5–75 °C) for 10 min, followed by immediate cooling in an ice bath. The treated enzyme was added to the reaction mixture and the activities were measured at room temperature. Moreover, the K_m value of the substrate F16BP and the inhibitory constant (K_i) of the inhibitor AMP were determined by the addition of different final concentrations of F16BP (0, 1.875, 3.75, 7.5, 10, 15, 20, and 30 μM) or AMP (0, 23.44, 46.88, 93.75, 187.5, 375, 750, 1500, and 3000 μM) into the 1 mL reaction mixture, respectively. The kinetic parameters (V_{max}, $K_{0.5(F16BP,\ AMP)}$, and n_H) were calculated by curve fitting of the following equation: $V = [V_{max} \times (c)^{nH}]/[K_{0.5}^{nH} + (c)^{nH}]$, where V_{max} is the maximum rate, c is the substrate concentration, K is the Michaelis-Menton constant or inhibitory constant, and n_H is Hill coefficient (Yuan et al., 2017). In addition, the kinetic characterisation of FBPase in the presence of different concentrations of AMP (3.125, 6.25, 12.5, 25, and 50 μM) was tested.

2.5. Site-directed mutagenesis of cFBPase

Site-directed mutagenesis was performed according to the method described by Meng, Shen, Yang, Zhang, & Sheng (2014). The mutated plasmids for the cFBPase mutants, including R30T, D32E, F33L, N218Y, and M251L, were obtained by PCR. The PCR mixture (50 μL) contained 1 U HF *Pfu* DNA polymerase, 200 μM dNTP mix, reaction buffer (Promega Corporation, Madison, WI, USA), 20 ng template DNA (plasmid Pet32-FBP), and mutated primer pairs (Table S1). The PCR products were transformed into *E. coli* DMT competent cells (Transgen Biotech, Beijing, China) and the positive clones were cultured. The mutated plasmids were extracted and verified by sequencing. The successfully mutated plasmids were further transformed into *E. coli* BL21 (DE3) for protein expression. In addition, the constructed R30T mutated plasmid was used as a template to amplify the mutated plasmids R30T/D32E and R30T/F33L. The D32E mutated plasmid was used to amplify plasmid D32E/F33L. Lastly, R30T/D32E/F33L was amplified using R30T/D32E as the template. The expression and purification processes were conducted as mentioned in section 2.3. In addition, the enzymatic characteristics of the obtained mutants, including enzyme activities, K_m values of F16BP, and K_i values of AMP, were measured based on the methods mentioned in section 2.4.

2.6. Molecular docking analysis

The tertiary structures (PDB files) of the wild-type (WT) and nine mutant proteins were obtained from the online I-TASSER service. The ligands (Mol2 files), including F16BP and AMP, were downloaded from the ZINC database (https://zinc.docking.org/). Autodock 4.2 (The Scripps research institute, La Jolla, CA, USA) was used to perform the docking analysis (Zhang, Liu, Yang, Chen, & Jiao, 2017). A grid box of 60 × 60 × 60 points with a default resolution was applied, and the center of the grid box was set to the geometric center of the predicted binding pocket. The results were analysed by the binding energy and the number of hydrogen bonds. The visualisation of the docking results was performed using Pymol 2.3 (Schrödinger LLC, New York, NY, USA) (Yan, Zhang, Hu, & Ma, 2013).

3. Results and discussion

3.1. Cloning and analysis of VrFBP

The CDS of *VrFBP* was cloned based on the mung bean genome, and was identified as a single copy gene based on genome annotation and alignment. The length of obtained PCR product was 1023 bp (coding a putative protein of 341 amino acids) and the sequence was submitted to GenBank database (accession no.: MK469994). Based on the nucleotide sequence, a phylogenetic tree was developed and is shown in Fig. S1. *VrFBP* showed highest similarity (98.53%) with cytosolic FBPase from *Vigna angularis* (*VaFBP*, XM_017558026). Moreover, *VrFBP* shared more than 90% sequence identity with the *FBP*s from *Phaseolus vulgaris* (95.99%, *PvFBP*, XM_007143470), *Cajanus cajan* (92.56%, *CcaFBP*, XM_020376533), *Glycine* max (92.18%, *GmFBP*, NM_001255239), and *Abrus precatorius* (90.51%, *ApFBP*, XM_027507461), which all belong to the Fabaceae family. The results indicated that the cytosolic FBPases from these species might share the same ancestral gene. In addition, *VrFBP* presented lower similarities with *FBP*s from other plants, such as *Cicer arietinum* (77.77%, *CarFBP*, XM_004485475), and *Oryza sativa* (77.06%, *OsFBP*, XM_015785975). The phylogenetic relationships of the FBPase genes were consistent with the divergence time of the species used (http://www.timetree.org/) (Kumar, Stecher, Suleski, & Hedges, 2017).

3.2. Amino acid sequence analysis of cFBPase

The multiple alignment of amino acid sequences of cFBPase of mung bean and some typical FBPases is presented in Fig. 1A. The secondary structure analysis showed that the main chain of Vr-cFBPase comprised 8 α-helices and 16 β-strands (Fig. 1Ba). The functional sites, labeled by Conserved Domains analysis (https://www.ncbi.nlm.nih.gov/Structure/cdd/wrpsb.cgi), showed that the AMP binding site residues (Leu^{20}, Gln^{23}, Arg^{30}, Asp^{32}, Phe^{33}, Thr^{34}, Lys^{115}, and Tyr^{116}, ordered according to the Vr-cFBPase sequence) formed a pocket surface structure (Fig. 1Bc). However, these binding site residues were not conserved in different species. For example, the Leu^{20} in H1 was conserved in all selected plant FBPases, but not in the *E. coli* and human enzymes. Furthermore, an AMP binding domain composed of four continuous amino acid residues at the start of H2 exhibited high conservation among the selected plant cFBPases. However, the Arg^{30} in the cpFBPase from spinach, were replaced by Asp and Thr in the FBPases of *E. coli* and human, respectively. Moreover, replacements of Asp^{32} and Phe^{33} by Glu and Leu, respectively, were observed. Lastly, two binding site residues, Lys^{115} and Tyr^{116}, showed consistency among different species.

Thr^{27} and Glu^{29} in the human FBPase (Hs-FBPase) form hydrogen bonds with the phosphate part of AMP (Kelley-Loughnane & Kantrowitz, 2001). In addition, Thr^{31} contacts with the amino part, and Ala^{24}, which was replaced as Pro^{27} in Vr-cFBPase (Fig. 1A), forms van der Waals contact with the adenine part. The Hs-FBPase exhibited relative high affinity with the inhibitor AMP (K_i = around 6–9 μM, Table S2). In spinach cpFBPase (So-cpFBPase), the binding site Arg^{30} was replaced by Asp. These differences might result in lost AMP affinity (Daie, 1993). In addition, the cFBPase of spinach presented relative low affinity for AMP (K_i = around 120 μM). Similar results were observed for the pea cFBPase (Jang, Lee, Lee, & Hahn, 2003). The amino acid sequences of AMP binding sites in mung bean Vr-cFBPase showed high conservation compared with those in spinach cFBPase (So-cFBPase), indicating similar AMP binding properties between the two enzymes.

The predicted six metal binding site residues (Asp^{77}, Glu^{100}, Glu^{101}, Asp^{121}, Leu^{123}, and Glu^{283}) of Vr-cFBPase were all conserved in different species (Fig. 1A). For human and *E. coli* FBPases, Mg^{2+} or Mn^{2+} are required for the catalysis activity (Brown et al., 2009; Shi et al., 2013). A group of functional site residues including Glu^{97}, Glu^{98}, Asp^{118}, and Asp^{121}, in human liver FBPase forms a negatively charged binding pocket for divalent metal ions. These residues are also conserved in the pig kidney enzyme, indicating their important functions during evolution (El-Maghrabi, Gidh-Jain, Austin, & Pilkis, 1993). One of the metal sites is coordinated by Glu^{97}, Asp^{118}, Glu^{280}, and the 1-phosphate part of the substrate, and the other one is coordinated by Glu^{97}, Asp^{118}, Leu^{120}, and the substrate. Asp^{74} forms a crucial hydrogen bond with the C-

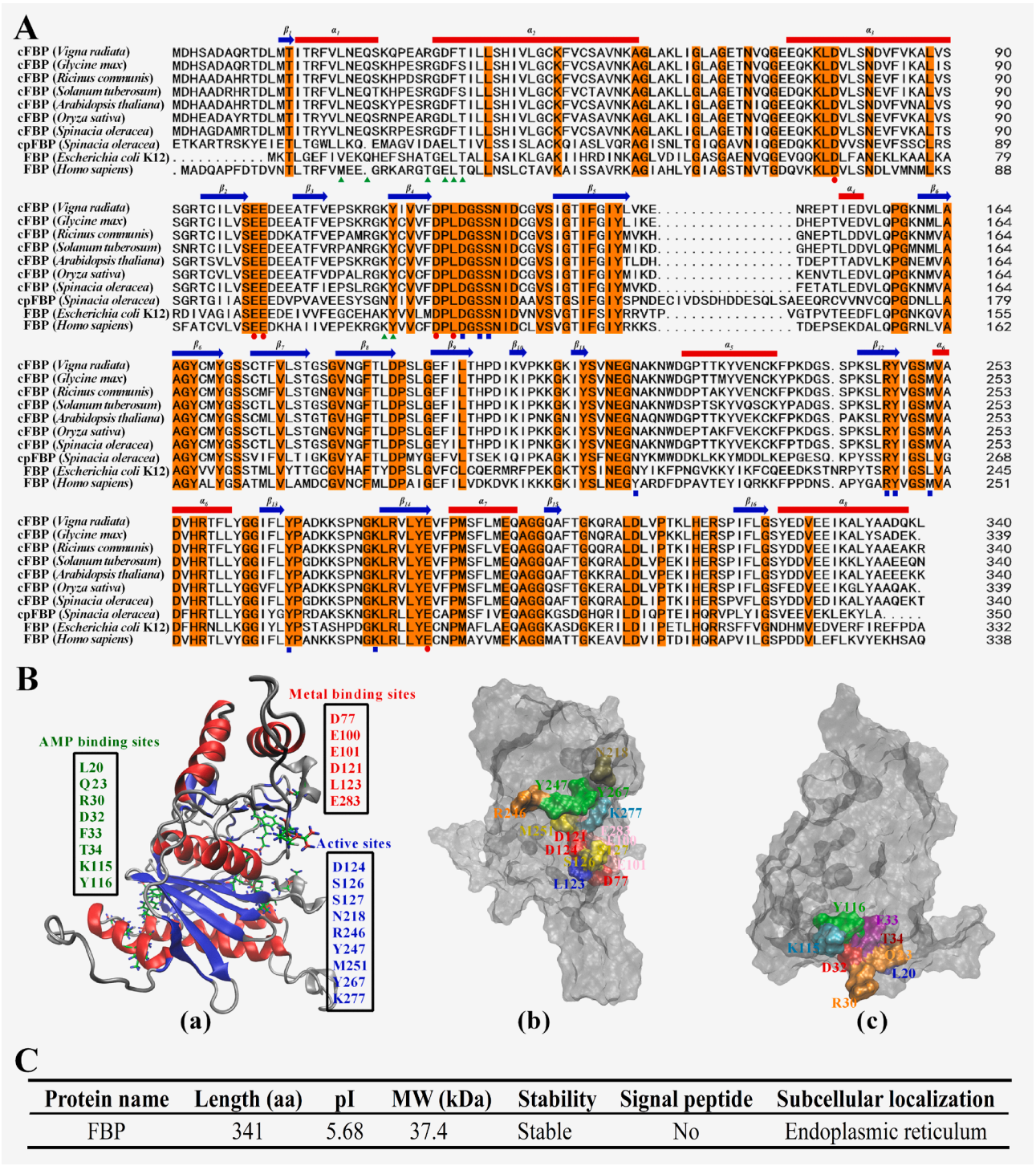

Protein name	Length (aa)	pI	MW (kDa)	Stability	Signal peptide	Subcellular localization
FBP	341	5.68	37.4	Stable	No	Endoplasmic reticulum

Fig. 1. A: Amino acid sequence alignment of selected fructose-1,6-bisphosphatases (FBPs). The sequences of FBPs from *Vigna radiata*, *Glycine* max, *Ricinus communis*, *Solanum tuberosum*, *Arabidopsis thaliana*, *Oryza sativa*, *Spinacia oleracea*, *Escherichia coli*, and *Homo sapiens*, are shown. The conserved amino acids in all selected species are highlighted in orange and residues marked by green triangles (▲), red circles (●), and blue squares (■) represent predicted adenosine monophosphate (AMP) binding sites, metal binding sites, and active sites, respectively. The secondary structures of FBP from *Vigna radiata* are shown above the sequence, and helices and strands are exhibited as red bars and blue arrows, respectively. B: A structural model of FBP from *Vigna radiata* obtained from homology modelling using the crystal structure of FBP from pig kidney (PDB code: 1FSA) as the template. C: The deduced polypeptide properties, including length, isoelectric point, molecular weight, stability index, signal peptide, and subcellular localisation. (For interpretation of the references to colour in this figure legend, the reader is referred to the web version of this article.)

terminal of loop 50–72, which plays an important role in metal cation binding (Gao, Shen, & Honzatko, 2014). The conserved amino acids of metal binding sites indicated that the analysed enzymes might share similiar metal binding mechanisms.

The metal binding and active site residues (Asp^{124}, Ser^{126}, Ser^{127}, Asn^{218}, Arg^{246}, Tyr^{247}, Met^{251}, Tyr^{267}, and Lys^{277}) formed a complex catalytic center on the opposite side to the AMP binding pocket (Fig. 1A, Bb). Of the nine predicted active site residues, 7 were consistent in the

10 selected FBPases. However, Asn^{218} was replaced by Tyr in the human enzyme, and it interacts with the 6-phosphate group of the substrate. Furthermore, Met^{251} was replaced by Leu in So-cpFBPase and Ec-FBPase, which binds to the furanose ring (Liang, Huang, Zhang, Ke, & Lipscomb, 1992). During the catalytic reaction, a proton is transferred from Asp^{121} (carboxyl group) of Hs-FBPase to the ester oxygen of the substrate (El-Maghrabi, Gidh-Jain, Austin, & Pilkis, 1993). The backbone NH of Ser^{123} and Ser^{124} might interact with the 1-phosphate of the substrate, F16BP. In addition, Tyr^{244}, Tyr^{264}, and Lys^{274} coordinately form hydrogen bonds with the 6-phosphate group (Liang, Huang, Zhang, Ke, & Lipscomb, 1992). The high proportion of conserved metal binding and active site residues in mung bean indicated that the catalysis mechanism and properties of Vr-cFBPase might be similar with the well-studied So-FBPase or Ec-FBPase.

The obtained protein model was verified using Ramachandran plot (Fig. S2) and Verify3D scores (Fig. S3). The results showed that 98.6% of residues located in the allowed area and 92.67% of the residues scored more than 0.2, indicating the reliability of the model. Furthermore, some basic molecular properties of Vr-cFBPase were predicted by related bioinformatic tools (Fig. 1C). The results showed that this protein contained 341 residues and the isoelectric point was around 5.68, which was higher than the cpFBPase in spinach (4.65) (Reichert, Dennes, Vetter, & Scheibe, 2003). Furthermore, the molecular weight (MW) of Vr-cFBPase was predicted as 37.4 kDa. Similarly, the MWs of cFBPases in both sugar beet and spinach are around 37 kDa (Daie, 1993). In addition, the FBPases from human and pig also show MWs at around 37 kDa (El-Maghrabi, Gidh-Jain, Austin, & Pilkis, 1993; Gao, Shen, & Honzatko, 2014). However, cpFBPases generally present larger MWs compared with cFBPases because of the inserted additional functional residues. According to the stability index value, the Vr-cFBPase protein was stable, with an instability index lower than 40 (Chen et al., 2015).

3.3. Purification and characterisation of Vr-cFBPase

The recombinant plasmid Pet32-FBP was expressed in BL21 (DE3) and induced by IPTG. The SDS-PAGE results (Fig. 2) showed that compared with the intracellular protein bands in uninduced group (lane U), the induced group (lane I) presented a higher band intensity corresponding to the predicted size of Vr-cFBPase (around 37 kDa). The crude cytoplasmic protein extract was further purified, and the purified protein was analysed using SDS-PAGE. A single band at 37 kDa was presented (lane WT), which was consistent with the predicted MW of the Vr-cFBPase in the vector. The results showed that Vr-cFBPase had a similar amino acid sequence and MW compared with those of other plants, indicating the conservative properties of this enzyme (Daie, 1993; Zhou & Cheng, 2004).

The Vr-cFBPase enzyme activities were monitored by measuring the contents of NADPH formed via the coupling glucose-6-phosphate dehydrogenase and phosphoglucose isomerase (Fig. 3). The metal requirement test showed that the Vr-cFBPase exhibited specific requirements for the divalent metal ions Mg^{2+} or Mn^{2+} (Fig. 3A). The enzyme did not show catalysing activity without metal ions. In addition, it had no requirement for other metal ions, including Ca^{2+}, Co^{2+}, Cu^{2+}, and Zn^{2+}, at the tested concentration range of 0.01–10 mM. Furthermore, under the same ion concentration (5 mM), the Vr-cFBPase showed higher affinity for Mn^{2+} compared with that for Mg^{2+}. The enzyme activity was 13.87 $\mu mol \cdot min^{-1} \cdot mg^{-1}$ in the Mn^{2+} group, while it was 3.66 $\mu mol \cdot min^{-1} \cdot mg^{-1}$ in the Mg^{2+} group. Furthermore, the enzymatic kinetics under different concentrations of metal ions showed that the enzyme responded to Mg^{2+} and Mn^{2+} with a K_m of 1.72 and 6.07 mM, respectively (Fig. 3B). These results are consistent with a previous study of cFBPase from apple leaf (Zhou & Cheng, 2004). Either Mn^{2+} or Mg^{2+} was needed for the enzyme activity, with a K_m value of 62 μM and 0.59 mM, respectively. However, some different metal requirements were found in other FBPases. For example, the pig kidney FBPase could be activated by Zn^{2+}. In addition, a metal-independent FBPase was found in *Saccharomyces cerevisiae* (Kuznetsova et al., 2010).

The thermal stability of Vr-cFBPase was studied and the results showed that the enzyme maintained relatively high activities at low temperatures (5, 15, and 25 °C) (Fig. 3C). The activity was reduced to 6.26 $\mu mol \cdot min^{-1} \cdot mg^{-1}$ after pre-treatment at 35 °C for 10 min. Moreover, the enzyme activity decreased continuously as the temperature increased, and was almost completely inactivated at temperatures higher than 65 °C. The results indicated that heat treatment could not be applied in the purification of recombinant Vr-cFBPase (Jang, Lee, Lee, & Hahn, 2003). In addition, the catalysing kinetics of Vr-cFBPase substrate (F16BP) were monitored (Fig. 3D). The results showed that F16BP bound to Vr-cFBPase by positive cooperativity with a Hill coefficient value of 3.19. The conclusion was consistent with the study of FBPase in *Leishmania* (Yuan et al., 2017). The K_m value of 7.96 μM was similar to those of pig kidney FBPase (1.4–5.9 μM), and human FBPase (0.8–3.3 μM) (Table S2) (Ludwig et al., 2007). The results might be explained by the replacement of the active site Asn^{218} (Fig. 1A), resulting in similar contact with the 6-phosphate group of F16BP (discussed later in site-directed mutagenesis part).

AMP inhibits the FBPase activity by binding to sites that are about 30 Å distant from the active site. Its allosteric inhibition mechanism in mammals has been well studied (Yuan et al., 2017). In this study, the inhibitive effect of AMP on cFBPase was tested and is presented in Fig. 3E. The K_i value of Vr-cFBPase was 111.09 μM and the n_H was 0.91, indicating negatively cooperative binding. Interestingly, the data in

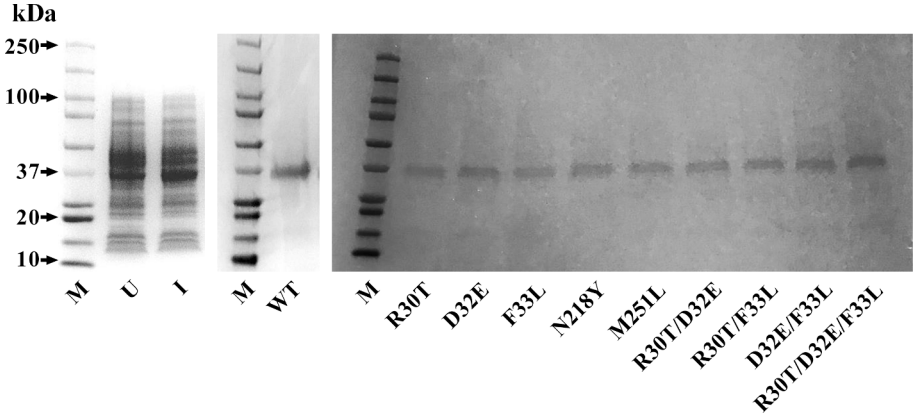

Fig. 2. Sodium dodecyl sulphate polyacrylamide gel electrophoresis (SDS-PAGE) analysis of fructose-1,6-bisphosphatase extracts. Lane M: Protein markers from 10 to 250 kDa; Lane U: uninduced cytoplasmic total proteins; Lane I: induced cytoplasmic total proteins; Lane WT, R30T, D32E, F33L, N218Y, M251L, R30T/D32E, R30T/F33L, D32E/F33L, and R30T/D32E/F33L: purified wild-type (WT) and mutant proteins.

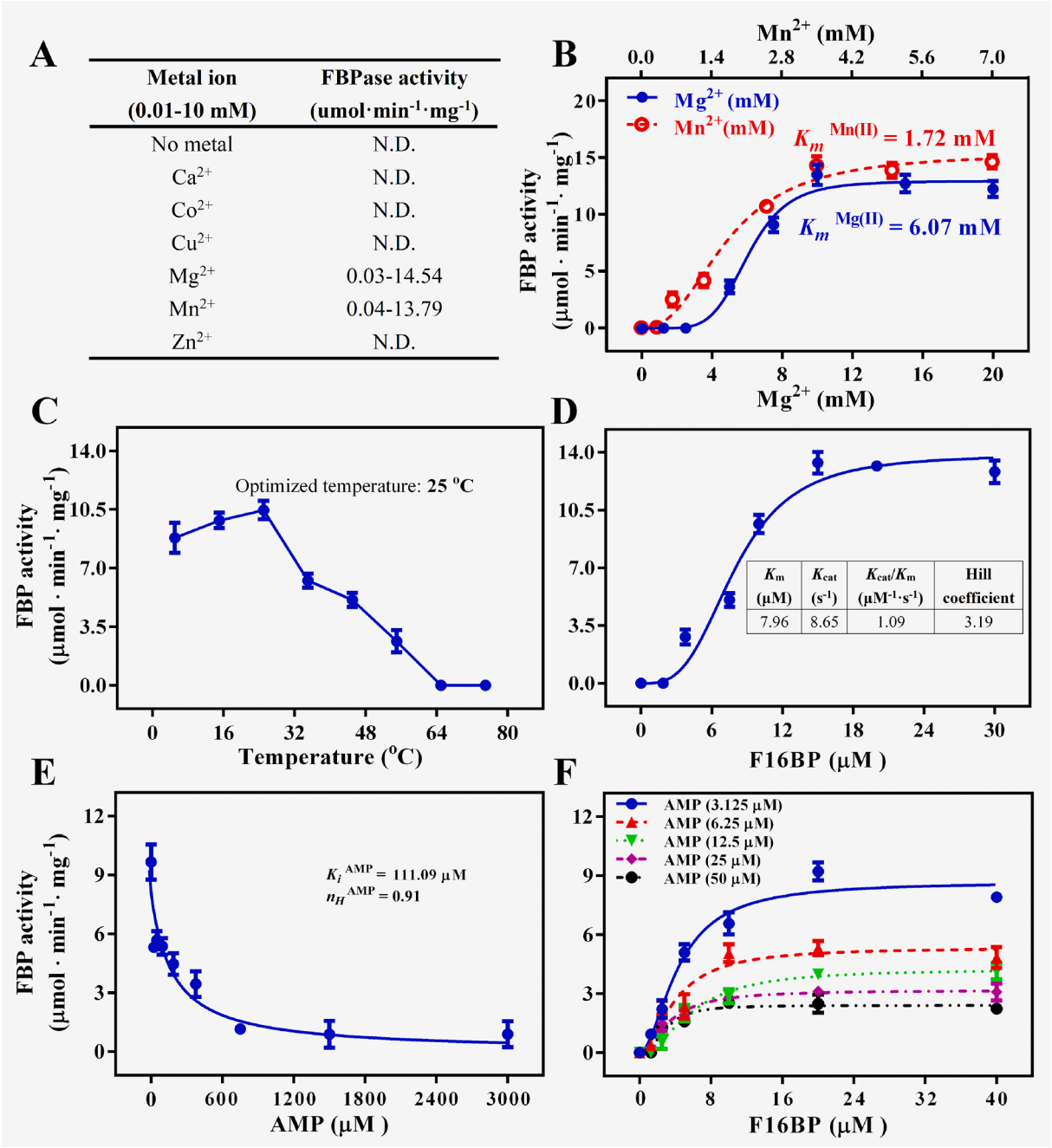

Fig. 3. A: Metal ion requirement test of mung bean fructose-1,6-bisphosphatase (Vr-cFBPase). B: Kinetic activities under different concentrations of Mg^{2+} and Mn^{2+}. C: Heat stability test of Vr-cFBPase. D: Enzyme activities under different concentrations of substrate fructose-1,6-bisphosphate (F16BP). E: Enzyme activities in the presence of different concentrations of inhibitor adenosine monophosphate (AMP). F: Kinetic characterisation of Vr-cFBPase under different concentrations of AMP.

Table S2 showed that the AMP K_i values of cFBPases from different plants are generally equivalent, at around 120 μM. By contrast, the FBPases for mammals had significantly lower K_i values (2.8–24 μM) (Daie, 1993; Dżugaj & Kochman, 1980; Gidh-Jain et al., 1994; Jang, Lee, Lee, & Hahn, 2003; Kelley, Giroux, Lu, & Kantrowitz, 1996; Kelley-Loughnane et al., 2002; Liu & Fromm, 1988; Ludwig et al., 2007; Opheim & Bernlohr, 1975). Sequence analysis showed that, compared with those in Hs-FBPase, the AMP binding site residues of cFBPases in the selected plants were poorly conserved (Fig. 1A), with only two (Lys^{115} and Tyr^{116}) being identical out of eight residues. The differences in residue sequences explain the weaker AMP binding affinity of these cFBPases (lower K_i values). The determined K_i value (111.09 μM) of Vr-cFBPase is likely to be in the physiological range of intracellular AMP levels in mung bean revealed in our previous study (estimated as 105–469 μM) (Chen, Tan, Zhao, Yang, & Yang, 2019). This suggested that Vr-cFBPase and its related metabolism might be regulated by the AMP content in mung bean. The activity kinetic curves of Vr-cFBPase in the presence of different AMP contents showed that the maximum activity decreased as AMP concentration increased (Fig. 3F). In addition, the substrate (F16BP) affinity was not altered under different AMP levels, confirming that Vr-cFBPase is noncompetitively inhibited by AMP.

3.4. *Site-directed mutagenesis and molecular docking analysis*

Based on the sequence and activity studies, five functional site

residues, including three AMP binding site residues (Arg^{30}, Asp^{32} and Phe^{33}) and two active site residues (Asn^{218} and Met^{251}) were mutated using site-directed mutagenesis. Moreover, four combined mutants were generated to study the AMP binding properties of Vr-cFBPase. The constructed plasmids were verified by sequencing and the expressed proteins (R30T, D32E, F33L, N218Y, M251L, R30T/D32E, R30T/F33L, D32E/F33L, and R30T/D32E/F33L) were purified and checked by SDS-PAGE (Fig. 2). The substrate (F16BP) catalysing capacities of the ten proteins (WT and nine mutants) were determined and are shown in Fig. 4. The results showed that mutations of these functional sites resulted in changes to the maximum reaction rate and substrate affinity of Vr-cFBPase. Three mutants, R30T, N218Y, and R30T/D32E exhibited lower enzyme activities compared with that of the WT. By contrast, the activities of the other mutants were increased by different degrees. For example, the D32E/D33L mutant presented the highest catalysis rate, of 33.36 μmol·min^{-1}·mg^{-1}. The replacement of Met^{251} by Leu^{251} improved the enzyme activity by 13.87%. In addition, the changes to the binding affinities (K_m) of the mutants generally exhibited a negative correlation with the altered enzyme activities. For instance, the K_m values of D32E/D33L and M251L decreased from 8.12 μM (WT) to 3.78 and 2.53 μM, respectively.

Mutation (N218Y) of active site Asn^{218} in Vr-cFBPase did not significantly affect the K_m value compared with that of the WT. The results indicated that the amino acid Tyr, which contacts with the 6-phosphate of substrate (Liang, Huang, Zhang, Ke, & Lipscomb, 1992), might be replaceable by Asn and might share a similar binding mechanism in FBPases. This explained the similar substrate catalysing properties between Vr-cFBPase and Hs-FBPase. Contrastingly, M251L presented significantly higher activity and affinity. Met^{251} is conserved in cFBPases and Hs-FBPase, and it is replaced by Leu in cpFBPase and Ec-FBPase (Fig. 1). The mutation results indicated that residue replacement might result in conformational and/or affinity alterations of the enzyme. Further molecular docking analysis showed that the hydrogen bonds formed by Tyr^{247} and Lys^{277} might play an important role in the substrate binding property of Vr-cFBPase (Fig. 5A). Although Met^{251} does not directly bind with the substrate F16BP, the binding energy of M251L decreased from − 1.73 (WT) to − 2.58 kcal·mol^{-1}, and the molecular distance between the active site and ligand was lowered from 4.9 to 4.2 Å (Fig. 5B). These results explained the improved affinity and activity of M251L compared with that of the WT. Interestingly, mutations of AMP binding site residues also affected the F16BP catalysing property of Vr-cFBPase. Around three times higher enzyme activity was observed for the R30T/D32E mutant. Docking analysis showed that the binding energy was decreased to − 1.97 kcal·mol^{-1} (Fig. 5C). The results indicated that the mutations of Asp^{32} and Phe^{33}, which are located at the endpoint of H2, might change the protein's conformation and further improve the activity and affinity of Vr-cFBPase. A previous study also showed that the alteration of AMP binding site residues (Lys^{112} and Tyr^{113}) of FBPase (pig kidney) resulted in an increased K_m and reduced Mg^{2+} affinity (Kelley-Loughnane & Kantrowitz, 2001). These results revealed the allosteric property of FBPase and suggested a direct connection between the AMP binding pocket and the active site.

The functional properties of selected AMP binding site residues were also studied using site-directed mutagenesis and molecular docking (Fig. 6). The continuous Arg^{30}, Asp^{32}, Phe^{33}, and Thr^{34} form an important component in the AMP binding pocket and the binding mechanisms of their homologous residues in human and pig have been studied extensively (Kelley-Loughnane & Kantrowitz, 2001). In this study, the non-conserved residues Arg^{30}, Asp^{32}, and Phe^{33} in Vr-cFBPase were replaced by the corresponding amino acids from Hs-FBPase. The AMP affinities of the WT and the related mutants are shown in Fig. 6A. The WT exhibited a K_i value around 120 μM, which was similar with the

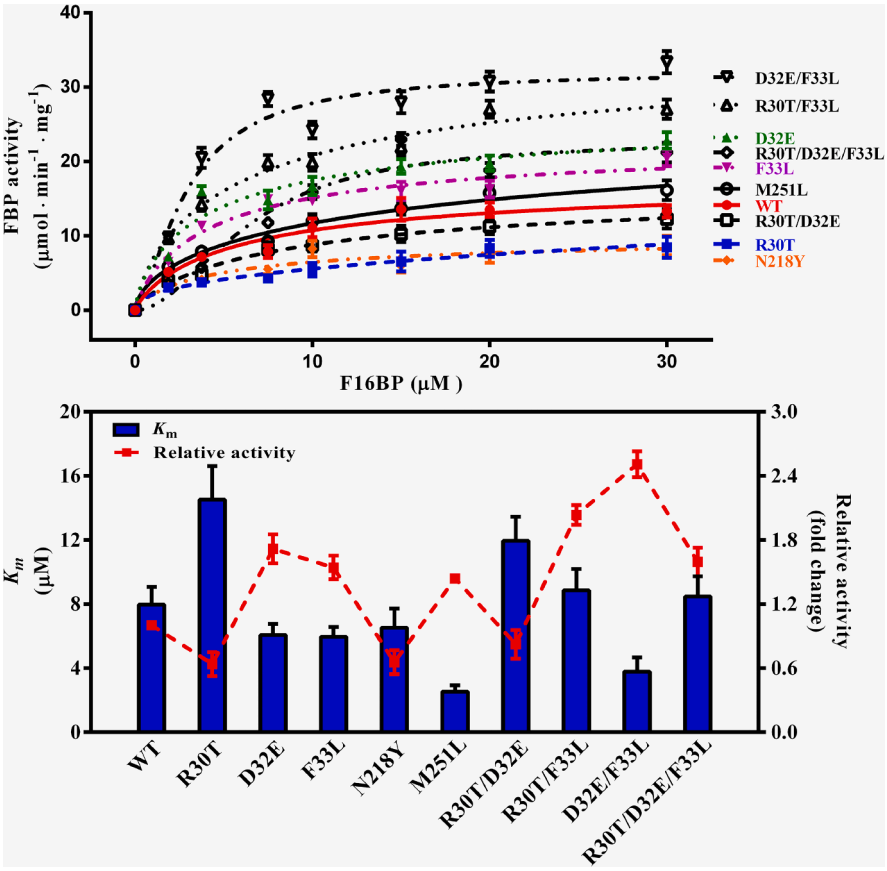

Fig. 4. A: Kinetic activities of the wild-type (WT) mung bean fructose-1,6-bisphosphatase (Vr-cFBPase) and nine mutants. B: The Michaelis-Menton constant (K_m) and relative activity of each protein.

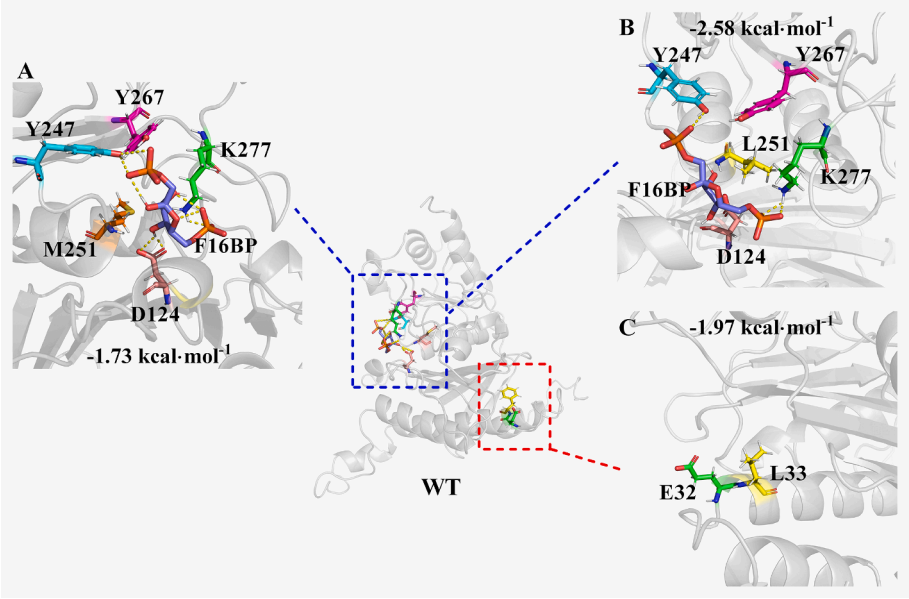

Fig. 5. Molecular docking analysis of wild-type mung bean fructose-1,6-bisphosphatase (Vr-cFBPase) (WT, A), the M251L mutant (B), and the D32E/F33L mutant (C).

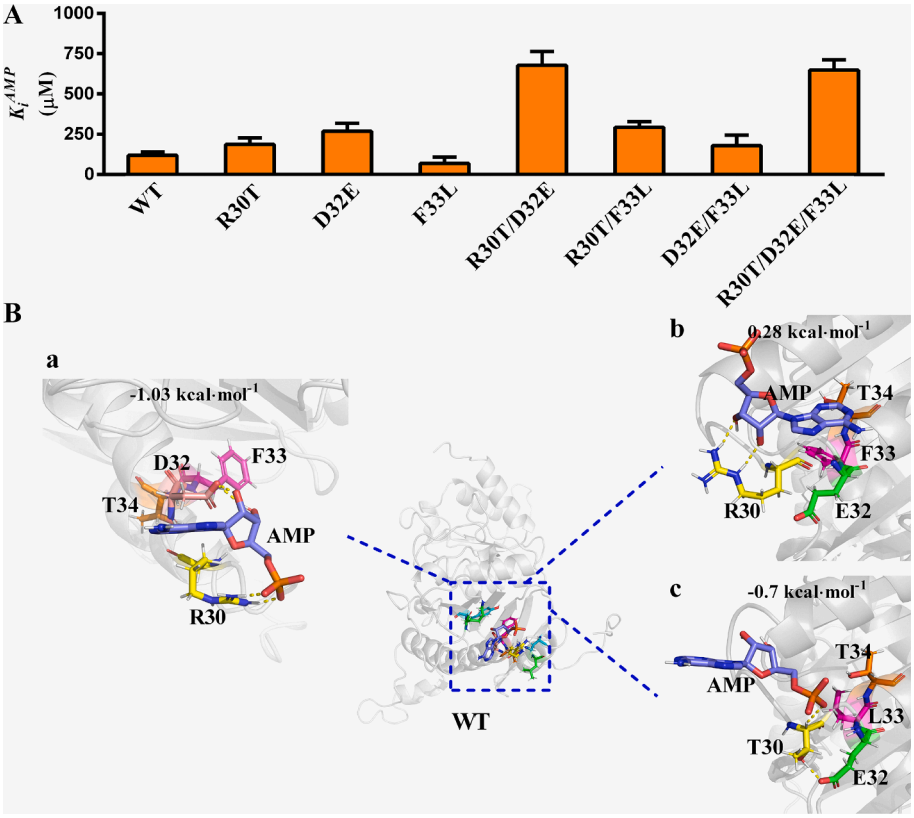

Fig. 6. A: Adenosine monophosphate (AMP) inhibitory constant (K_i) of each protein. B: Molecular docking analysis of wild-type mung bean fructose-1,6-bisphosphatase (Vr-cFBPase) (WT, a), the D32E mutant (b), and the R30T/D32E/F33L mutant (c).

cFBPases in pea and spinach (Table S2). Docking analysis showed that Arg^{30} and Asp^{32} formed hydrogen bonds with AMP and the binding energy was − 1.03 kcal·mol^{-1} (Fig. 6Ba). The results were consistent with the homologous sites in the human enzyme (Kelley-Loughnane & Kantrowitz, 2001). Compared with the WT, most of the mutants (except F33L) exhibited higher K_i values, indicating weakened binding affinities for AMP.

Of the single residue mutants (R30T, D32E, and F33L), D32E presented highest K_i value (268.39 μM). In addition, the combined mutants R30T/D32E and R30T/D32E/F33L showed higher K_i values (678.39 and 649.03 μM, respectively) among the mutants. These results indicated that Asp^{32} might play an important role in maintaining the binding affinity of Vr-cFBPase. Molecular docking showed that the hydrogen bond between Asp^{32} and AMP disappeared after residue replacement by Glu

(Fig. 6Bb). However, in the human FBPase, the homologous residue (Glu^{29}) forms a hydrogen bond with AMP and exhibited low Ki values (6–9 μM) (Dżugaj & Kochman, 1980; Gidh-Jain et al., 1994; Kelley-Loughnane & Kantrowitz, 2001). The results indicated that plant evolved a discriminative AMP binding conformation compared with that in the human enzyme. In addition, the binding energy of D32E was improved to 0.28 kcal·mol^{-1}. The molecular distance between the enzyme and AMP was increased from 5.1 (WT) to 8.0 Å (D32E). These data helped to explain the decreased AMP affinity of the D32E mutant. In addition, docking analysis of R30T/D32E/F33L showed that the replaced Thr^{30} formed a hydrogen bond with AMP (Fig. 6Bc). Furthermore, the binding energy and molecular distance were improved to −0.7 kcal·mol^{-1} and 11.9 Å, respectively, compared with those of the WT. The docking results were generally in accordance with the K_i analysis of the purified proteins. Although Hs-FBPase exhibited higher AMP binding affinity than Vr-cFBPase (Table S2), the replacement of selected binding site residues in Vr-cFBPase by the homologous residues in Hs-FBPase could not enhance the AMP binding affinity of Vr-cFBPase. This implied that the evolved AMP binding sites of mung bean cFBPase are interconnected and coordinately form the binding conformation. The functional characteristics of cFBPase active site residues provide reference information for our further genome editing study of mung bean.

4. Conclusion

The goals of this study were to structurally characterise the cFBPase of mung bean, and eventually improve the crop quality and yield. The CDS (MK469994) of cFBPase from mung bean was firstly cloned. Some basic bioinformatic analyses (phylogenetic tree, secondary structure prediction, homology modelling, isoelectric point, etc.) were conducted to obtain general information about the Vr-cFBPase. The protein was expressed, purified, and further characterised. Vr-cFBPase is around 37 kDa and exhibited divalent metal ion requirements of Mg^{2+} and Mn^{2+} at a concentration range of 0.01–10 mM. The K_m values of Mg^{2+} and Mn^{2+} for enzyme activation were 1.72 and 6.07 mM, respectively. Moreover, the Vr-cFBPase was not heat stable and its K_m and K_i values of the substrate F16BP and inhibitor AMP were 7.96 and 111.09 μM, respectively. In addition, the functional properties of selected residues were studied using site-directed mutagenesis and molecular docking analysis. The results showed that the active site residues Asn^{218} and Met^{251} in Vr-cFBPase could be replaced by homologous Tyr and Leu, respectively, and that the M251L mutant resulted in improved enzyme activity and substrate affinity. The decreased binding energy and molecular distance might contribute to the alteration. Furthermore, mutations of AMP binding site residues also affected the enzyme's activities, indicating the connection between the AMP binding site and the active site. Lastly, the K_i of the mutants revealed the important role of Asp^{32} in Vr-cFBPase's affinity for AMP. This work provides valuable information for the structural properties of cFBPase, and lays the foundation for further precision breeding of mung bean.

CRediT authorship contribution statement

Lin Chen: Conceptualization, Methodology, Investigation, Writing - original draft. **Xue Zhao:** Conceptualization, Software, Investigation. **Yun He:** Methodology, Validation. **Hongshun Yang:** Conceptualization, Funding acquisition, Project administration, Supervision, Writing - review & editing.

Declaration of Competing Interest

The authors declare that they have no known competing financial interests or personal relationships that could have appeared to influence the work reported in this paper.

Acknowledgements

This study was funded by Natural Science Foundation of Jiangsu Province (BK20181184), the Singapore Ministry of Education Academic Research Fund Tier 1 (R-160-000-A40-114), projects 31371851 and 31071617 supported by NSFC, and an industry grant supported by Changzhou Qihui Management & Consulting Co., Ltd (R-160-000-A82-597).

Appendix A. Supplementary data

Supplementary data to this article can be found online at https://doi.org/10.1016/j.foodchem.2020.128973.

References

Brown, G., Singer, A., Lunin, V. V., Proudfoot, M., Skarina, T., Flick, R., Kochinyan, S., Sanishvili, R., Joachimiak, A., Edwards, A. M., Savchenko, A., & Yakunin, A. F. (2009). Structural and Biochemical Characterization of the Type II Fructose-1,6-bisphosphatase GlpX from *Escherichia coli*. *Journal of Biological Chemistry, 284*(6), 3784–3792. https://doi.org/10.1074/jbc.M808186200.

Chen, L., Tan, J. T. G., Zhao, X., Yang, D., & Yang, H. (2019). Energy regulated enzyme and non-enzyme-based antioxidant properties of harvested organic mung bean sprouts (*Vigna radiata*). *LWT-Food Science and Technology, 107*, 228–235. https://doi.org/10.1016/j.lwt.2019.03.023.

Chen, L., Wu, Ji'en, Li, Z., Liu, Q., Zhao, X., & Yang, H. (2019). Metabolomic analysis of energy regulated germination and sprouting of organic mung bean (*Vigna radiata*) using NMR spectroscopy. *Food Chemistry, 286*, 87–97. https://doi.org/10.1016/j.foodchem.2019.01.183.

Chen, L., Yang, Y., Liu, C., Zheng, Y., Xu, M., Wu, N.a., Sheng, J., & Shen, L. (2015). Characterization of WRKY transcription factors in *Solanum lycopersicum* reveals collinearity and their expression patterns under cold treatment. *Biochemical and Biophysical Research Communications, 464*(3), 962–968. https://doi.org/10.1016/j.bbrc.2015.07.085.

Cheng, F., Sheng, J., Dong, R., Men, Y., Gan, L., & Shen, L. (2012). Novel Xylanase from a Holstein Cattle Rumen Metagenomic Library and Its Application in Xylooligosaccharide and Ferulic Acid Production from Wheat Straw. *Journal of Agriculture and Food Chemistry, 60*(51), 12516–12524. https://doi.org/10.1021/jf302337w.

Daie, J. (1993). Cytosolic fructose-1,6-bisphosphatase: A key enzyme in the sucrose biosynthetic pathway. *Photosynthesis Research, 38*(1), 5–14. https://doi.org/10.1007/BF00015056.

Dżugaj, A., & Kochman, M. (1980). Purification of human liver fructose-1,6-bisphosphatase. *Biochimica et Biophysica Acta (BBA) - Enzymology, 614*(2), 407–412. https://doi.org/10.1016/0005-2744(80)90230-2.

El-Maghrabi, M. R., Gidh-Jain, M., Austin, L., & Pilkis, S. (1993). Isolation of a human liver fructose-1,6-bisphosphatase cDNA and expression of the protein in *Escherichia coli*. Role of ASP-118 and ASP-121 in catalysis. *Journal of Biological Chemistry, 268*(13), 9466–9472.

Gao, Y., Shen, L.u., & Honzatko, R. B. (2014). Central Cavity of Fructose-1,6-bisphosphatase and the Evolution of AMP/Fructose 2,6-bisphosphate Synergism in Eukaryotic Organisms. *Journal of Biological Chemistry, 289*(12), 8450–8461. https://doi.org/10.1074/jbc.M114.548586.

Gidh-Jain, M., Zhang, Y., Van Poelje, P. D., Liang, J. Y., Huang, S., Kim, J., … El-Maghrabi, M. R. (1994). The allosteric site of human liver fructose-1,6-bisphosphatase. Analysis of six AMP site mutants based on the crystal structure. *Journal of Biological Chemistry, 269*, 27732–27738.

Gütle, D. D., Roret, T., Müller, S. J., Couturier, J., Lemaire, S. D., Hecker, A., Dhalleine, T., Buchanan, B. B., Reski, R., Einsle, O., & Jacquot, J.-P. (2016). Chloroplast FBPase and SBPase are thioredoxin-linked enzymes with similar architecture but different evolutionary histories. *Proceedings of the National academy of Sciences of the United States of America, 113*(24), 6779–6784. https://doi.org/10.1073/pnas.1606241113.

Jang, H.-K., Lee, S.-W., Lee, Y.-H., & Hahn, T.-R. (2003). Purification and characterization of a recombinant pea cytoplasmic fructose-1,6-bisphosphatase. *Protein Expression and Purification, 28*(1), 42–48. https://doi.org/10.1016/S1046-5928(02)00654-X.

Kang, Y. J., Kim, S. K., Kim, M. Y., Lestari, P., Kim, K. H., Ha, B.-K., Jun, T. H., Hwang, W. J., Lee, T., Lee, J., Shim, S., Yoon, M. Y., Jang, Y. E., Han, K. S., Taeprayoon, P., Yoon, N.a., Somta, P., Tanya, P., Kim, K. S., Gwag, J.-G., Moon, J.-K., Lee, Y.-H., Park, B.-S., Bombarely, A., Doyle, J. J., Jackson, S. A., Schafleitner, R., Srinives, P., Varshney, R. K., & Lee, S.-H. (2014). Genome sequence of mungbean and insights into evolution within *Vigna* species. *Nature Communications, 5*(1). https://doi.org/10.1038/ncomms6443.

Kelley, N., Giroux, E. L., Lu, G., & Kantrowitz, E. R. (1996). Glutamic Acid Residue 98 Is Critical for Catalysis in Pig Kidney Fructose-1,6-bisphosphatase. *Biochemical and Biophysical Research Communications, 219*(3), 848–852. https://doi.org/10.1006/bbrc.1996.0321.

Kelley-Loughnane, N., Biolsi, S. A., Gibson, K. M., Lu, G., Hehir, M. J., Phelan, P., & Kantrowitz, E. R. (2002). Purification, kinetic studies, and homology model of *Escherichia coli* fructose-1,6-bisphosphatase. *Biochimica et Biophysica Acta (BBA) -*

Protein Structure and Molecular Enzymology, 1594(1), 6–16. https://doi.org/10.1016/S0167-4838(01)00261-8.

Kelley-Loughnane, N., & Kantrowitz, E. R. (2001). AMP inhibition of pig kidney fructose-1,6-bisphosphatase. *Biochimica et Biophysica Acta (BBA) - Protein Structure and Molecular Enzymology, 1548*(1), 66–71. https://doi.org/10.1016/S0167-4838(01)00218-7.

Kumar, S., Stecher, G., Suleski, M., & Hedges, S. B. (2017). TimeTree: a resource for timelines, timetrees, and divergence times. Molecular Biology and Evolution, 34(7), 1812-1819.

Kuznetsova, E., Xu, L., Singer, A., Brown, G., Dong, A., Flick, R., Cui, H., Cuff, M., Joachimiak, A., Savchenko, A., & Yakunin, A. F. (2010). Structure and Activity of the Metal-independent Fructose-1,6-bisphosphatase YK23 from *Saccharomyces cerevisiae*. *Journal of Biological Chemistry, 285*(27), 21049–21059. https://doi.org/10.1074/jbc.M110.118315.

Liang, J. Y., Huang, S., Zhang, Y., Ke, H., & Lipscomb, W. N. (1992). Crystal structure of the neutral form of fructose 1,6-bisphosphatase complexed with regulatory inhibitor fructose 2,6-bisphosphate at 2.6-A resolution. *Proceedings of the National Academy of Sciences, 89*(6), 2404–2408. https://doi.org/10.1073/pnas.89.6.2404.

Liu, F., & Fromm, H. J. (1988). Purification and characterization of fructose-1,6-bisphosphatase from bovine brain. *Archives of Biochemistry and Biophysics, 260*(2), 609–615. https://doi.org/10.1016/0003-9861(88)90488-2.

H.C. Ludwig F.N. Pardo J.L. Asenjo M.A. Maureira A.J. Yañez J.C. Slebe Unraveling multistate unfolding of pig kidney fructose-1,6-bisphosphatase using single tryptophan mutants: Selective GdmCl disruption of FBPase C1-C2 interface 274 20 2007 5337 5349 10.1111/j.1742-4658.2007.06059.x.

Meng, D., Shen, L., Yang, R., Zhang, X., & Sheng, J. (2014). Identification and active site analysis of the 1-aminocyclopropane-1-carboxylic acid oxidase catalysing the synthesis of ethylene in *Agaricus bisporus*. *Biochimica et Biophysica Acta (BBA) - General Subjects, 1840*(1), 120–128. https://doi.org/10.1016/j.bbagen.2013.08.030.

Ogawa, T., Kimura, A., Sakuyama, H., Tamoi, M., Ishikawa, T., & Shigeoka, S. (2015). Characterization and physiological role of two types of chloroplastic fructose-1,6-bisphosphatases in Euglena gracilis. *Archives of Biochemistry and Biophysics, 575*, 61–68. https://doi.org/10.1016/j.abb.2015.04.002.

Opheim, D. J., & Bernlohr, R. W. (1975). Purification and regulation of fructose-1,6-bisphosphatase from *Bacillus licheniformis*. *Journal of Biological Chemistry, 250*, 3024–3033.

Ozaki, K., Uchida, A., Takabe, T., Shinagawa, F., Tanaka, Y., Takabe, T., Hayashi, T., Hattori, T., Rai, A. K., & Takabe, T. (2009). Enrichment of sugar content in melon fruits by hydrogen peroxide treatment. *Journal of Plant Physiology, 166*(6), 569–578. https://doi.org/10.1016/j.jplph.2008.08.007.

Reichert, A., Dennes, A., Vetter, S., & Scheibe, R. (2003). Chloroplast fructose 1,6-bisphosphatase with changed redox modulation: Comparison of the *Galdieria* enzyme with cysteine mutants from spinach. *Biochimica et Biophysica Acta (BBA) - Proteins and Proteomics, 1645*(2), 212–217. https://doi.org/10.1016/S1570-9639(02)00539-3.

Rojas-González, J. A., Soto-Súarez, M., García-Díaz, Á., Romero-Puertas, M. C., Sandalio, L. M., Mérida, Á., Thormählen, I., Geigenberger, P., Serrato, A. J., & Sahrawy, M. (2015). Disruption of both chloroplastic and cytosolic FBPase genes results in a dwarf phenotype and important starch and metabolite changes in Arabidopsis thaliana. Journal of Experimental Botany, 66(9), 2673-2689.

R. Shi Z.-Y. Chen D.-W. Zhu C. Li Y. Shan G. Xu S.-X. Lin A. Hofmann Crystal Structures of Human Muscle Fructose-1,6-Bisphosphatase: Novel Quaternary States, Enhanced AMP Affinity, and Allosteric Signal Transmission Pathway PLoS ONE 8 9 e71242 10.1371/journal.pone.0071242.t002.

Tamoi, M., Hiramatsu, Y., Nedachi, S., Otori, K., Tanabe, N., Maruta, T., & Shigeoka, S. (2011). Increase in the activity of fructose-1,6-bisphosphatase in cytosol affects sugar partitioning and increases the lateral shoots in tobacco plants at elevated CO_2 levels. *Photosynthesis Research, 108*(1), 15–23. https://doi.org/10.1007/s11120-011-9645-1.

Villeret, V., Huang, S., Zhang, Y., Xue, Y., & Lipscomb, W. N. (1995). Crystal structure of spinach chloroplast fructose-1,6-bisphosphatase at 2.8. ANG. resolution. *Biochemistry, 34*(13), 4299–4306.

Yan, J., Zhang, G., Hu, Y., & Ma, Y. (2013). Effect of luteolin on xanthine oxidase: Inhibition kinetics and interaction mechanism merging with docking simulation. *Food Chemistry, 141*(4), 3766–3773. https://doi.org/10.1016/j.foodchem.2013.06.092.

Yuan, M., Vásquez-Valdivieso, M. G., McNae, I. W., Michels, P. A. M., Fothergill-Gilmore, L. A., & Walkinshaw, M. D. (2017). Structures of Leishmania Fructose-1,6-Bisphosphatase Reveal Species-Specific Differences in the Mechanism of Allosteric Inhibition. *Journal of Molecular Biology, 429*(20), 3075–3089. https://doi.org/10.1016/j.jmb.2017.08.010.

Zhang, C.-L., Liu, J.-C., Yang, W.-B., Chen, D.-L., & Jiao, Z.-G. (2017). Experimental and molecular docking investigations on the inclusion mechanism of the complex of phloridzin and hydroxypropyl-β-cyclodextrin. *Food Chemistry, 215*, 124–128. https://doi.org/10.1016/j.foodchem.2016.07.155.

Zhou, R., & Cheng, L. (2004). Biochemical characterization of cytosolic fructose-1,6-bisphosphatase from apple (Malus domestica) leaves. Plant and Cell Physiology, 45 (7), 879-886.